LIMNOLOGY and OCEANOGRAPHY: METHODS

ASLO

Limnol. Oceanogr.: Methods 18, 2020, 424–436

doi: 10.1002/lom3.10373

Air–water gas exchange in lakes and reservoirs measured from a moving platform by underwater eddy covariance

Peter Berg,* **Michael L. Pace**, **Cal D. Buelo**
Department of Environmental Sciences, University of Virginia, Charlottesville, Virginia, USA

Abstract

Air–water exchange rates of gasses, such as O_2, CO_2, and CH_4, are widely used in ecosystem studies of lakes and reservoirs, but their magnitudes are often difficult to assess. In this proof-of-concept study, we measured gas exchange by underwater eddy covariance in such lentic systems from a moving platform. We used an Acoustic Doppler Velocimeter and a fast-responding O_2-temperature sensor mounted in the bow of a boat to measure water velocity, O_2 concentration, and temperature below the air–water interface (~ 10 cm) while the boat was propelled at constant speed (~ 25 cm s^{-1}) by an electric trolling motor. Fluxes of O_2 and heat across the air–water interface and standard gas exchange coefficients, k_{600}, were calculated for every 3 min of traveled distance (~ 45 m). All deployments were done under calm low-wind conditions where empirical relationships for k_{600} are most uncertain. Deployment averages of k_{600} ranged from 0.070 to 0.39 m d^{-1} and were strongly correlated with both the heat flux and the water temperature. In one deployment, a > 20% variation in mean water column O_2 concentration was measured along a 1 km long transect of a reservoir. Given the typical size of O_2 concentration differences over the air–water interface that drive gas exchange, such lateral variations can, even at a near-constant exchange coefficient, result in highly biased whole-ecosystem fluxes if based on stationary single-point O_2 measurements. "Mobile" aquatic eddy covariance measurements enable quantification of gas exchange in lakes and reservoirs under true in situ conditions and with high temporal and spatial resolution.

Estimates of gas exchange over the air–water interface in lakes and reservoirs are used to assess their metabolic activity (Hanson et al. 2004; Van de Bogert et al. 2007, 2012), their emission of greenhouse gasses (Cole et al. 2010; Raymond et al. 2013; Wilkinson et al. 2016), and their role in regional (Billett and Moore 2008) and global (Cole et al. 2007; Bastviken et al. 2011; Raymond et al. 2013) carbon budgets. Because lentic systems generally are metabolic hotspots (Hanson et al. 2004; Van de Bogert et al. 2007, 2012), they play a much greater role in regional and global carbon cycling than their area would otherwise suggest (Cole et al. 2007; Tranvik et al. 2009; Holgerson et al. 2017). This makes accurate assessments of lentic air–water exchange of gasses such as CO_2 and CH_4, and how they vary spatially and temporally, crucial for obtaining reliable land surface greenhouse gas budgets (Battin et al. 2009).

Gas exchange for lentic ecosystems is controlled by multiple state variables and complex physical processes on both sides of the air–water interface (Macintyre et al. 1995; MacIntyre et al. 2010), and temporal and spatial variability of these processes can be pronounced (Staehr et al. 2010; Schilder et al. 2013; Holgerson et al. 2017). This adds to the challenges of determining accurate site- and time-specific rates, and as a result, gas exchange is viewed among aquatic scientists as a primary source of uncertainty in many estimates for aquatic systems (Raymond and Cole 2001; Raymond et al. 2012; Dugan et al. 2016).

Over the last few decades, a number of approaches have been developed for measuring or estimating gas exchange rates for lentic ecosystems (Cole et al. 2010; Staehr et al. 2010; Read et al. 2012), and current understanding of lentic gas exchange is largely based on applying and comparing these approaches in numerous different systems and under widely varying field conditions. A common approach for smaller lakes and reservoirs relies on inert tracer additions, for example, SF_6 (Wanninkhof 1985; Cole et al. 2010), whereas floating chambers are often deployed in larger reservoirs, lakes, and estuaries (Marino and Howarth 1993). In a limited number of studies of large reservoirs and lakes, tower- or boat-mounted atmospheric eddy covariance systems have been used to measure air–water gas exchange (Jonsson et al. 2008; Mammarella et al. 2015; Czikowsky et al. 2018; Reed et al. 2018). Partly

*Correspondence: pb8n@virginia.edu

driven by the substantial and often challenging effort required to measure gas exchange rates at specific sites with any of these approaches, many studies have simply relied on general empirical or semiempirical relationships for the exchange coefficient produced by fitting measurements done in other aquatic systems (Raymond and Cole 2001; Borges et al. 2004; Cole et al. 2010). With the exception of atmospheric eddy covariance measurements, none of these approaches represent a direct way of determining gas exchange, as they rely on assumptions that often are difficult to assess or simply not fulfilled. A review of these approaches and the large differences they often reveal when compared, show that there is an urgent need for methodological advances on this subject (Staehr et al. 2010; Vachon et al. 2010; Heiskanen et al. 2014).

In benthic environments, the aquatic eddy covariance technique for measuring O_2 fluxes (Berg et al. 2003) has become a generally accepted and widely used approach (Long et al. 2015; Berg et al. 2017; Attard et al. 2019). The technique has several important advantages over other flux methods, including its noninvasive nature (Lorrai et al. 2010), high temporal resolution (Rheuban and Berg 2013), and its ability to integrate over a large benthic surface (Berg et al. 2007). One of the fundamental assumptions in traditional aquatic eddy covariance measurements from a fixed position above a benthic system is that the flux signal is transported across the sensors by a well-developed turbulent flow (Berg et al. 2003; Kuwae et al. 2006; Lorrai et al. 2010). Right below the air–water interface of typical lentic systems with near-stagnant water much of the time, this condition is not met. However, because of molecular diffusivities for sparingly soluble gases such as O_2, CO_2, CH_4, and N_2O in water are minute, molecular diffusion of these gasses is a highly ineffective transport mechanism (Broecker and Peng 1974). As a result, slow "lacy" advective or convective water movements, driven by winds or unstable density stratifications for example, are still the dominant form of vertical transport of gasses in surface waters. This hints that the vertical gas transport up toward or down away from the air–water interface in lakes and reservoirs can be quantified by moving eddy covariance sensors through the water right below the interface at a controlled speed.

This is the principle we set out to test in this proof-of-concept study in which we applied the aquatic eddy covariance technique for O_2 flux measurements "upside-down" right below the air–water interface from a moving platform in a reservoir with near-stagnant water. From these "mobile" measurements of O_2 fluxes, we derived standard gas exchange coefficients (k_{600}) that can easily be translated to any gas of interest and related their variations to variables such as concurrently measured heat fluxes and water temperatures. All deployments were done under calm low-wind conditions in which empirical relationships for k_{600} become increasingly uncertain or break down (Clark et al. 1995; Cole and Caraco 1998; Vachon et al. 2010).

Use materials and procedures

Mobile measurement platform

We tested a few platform designs, including a mobile version of the small platform used by Berg and Pace (2017) to measure gas exchange in rivers and streams. The one that gave the most consistent high-quality data was a two-person sports-fishing boat propelled by an electric trolling motor and stabilized with one or two water-filled ballast tanks as shown in Fig. 1. During deployments, it was easy to keep the boat moving on a steady course and at a constant speed.

Aquatic eddy covariance instruments

Using standard aquatic eddy covariance sensors mounted in the bow of the boat, we measured the three-dimensional (3D) water velocity field, O_2 concentration, and temperature below the air–water interface ($\sim$ 10 cm) while the boat was propelled at a constant speed ($\sim$ 25 cm s^{-1}). Using custom-made stainless steel brackets, these sensors were mounted between the pontoons of the boat (Fig. 1a,b) and far enough out in front of it to ensure that data recordings were not disturbed by the boat or its movement.

The 3D water velocity field was measured with an acoustic Doppler velocimeter (ADV) with a cabled sensor head (cabled Vector, Nortek AS). This type of ADV allowed the sensor head to be positioned facing upwards (Fig. 1a) while recording the velocity field right below the air–water interface. Data were recorded continuously at a rate of 64 Hz and represent the average water velocity for the ADV's cylindrical measuring volume (Ø $\sim$ 1.4 cm, $h \sim$ 1.4 cm) centered 15.7 cm above the sensor head (Fig. 1a).

The O_2 concentration was measured with a fast-responding dual O_2-temperature sensor that was developed specifically for aquatic eddy covariance measurements (Berg et al. 2016) and is now commercially available (RINKO EC, JFE Advantech). The sensor, as shown in Fig. 2, consists of a miniature planar optode with a 5.0 mm diameter O_2 sensing foil and a < 1 mm diameter thermistor positioned next to it. The distance between the center of the foil and the thermistor is $\sim$ 5 mm; the entire tip has a diameter of 8.0 mm, which makes it far more robust than Clark-type and optical fiber micro-sensors often used for aquatic eddy covariance measurements (Berg et al. 2017). The sensor was designed to interface with a standard ADV through a single cable supplying power to the sensor and also transmitting its two outputs, one for O_2 and one for temperature, to the ADV's data logger to be recorded along with the 3D water velocity field. Combined, these data allow parallel eddy fluxes of O_2 and sensible heat to be derived.

Because the O_2 signal and the temperature are measured within a few millimeters of one another (Fig. 2), the sensor allows for instantaneous temperature correction of the O_2 reading, which is critically important in air–water gas-exchange measurements (Berg and Pace 2017). All highly sensitive and fast-responding O_2 sensors are inherently sensitive

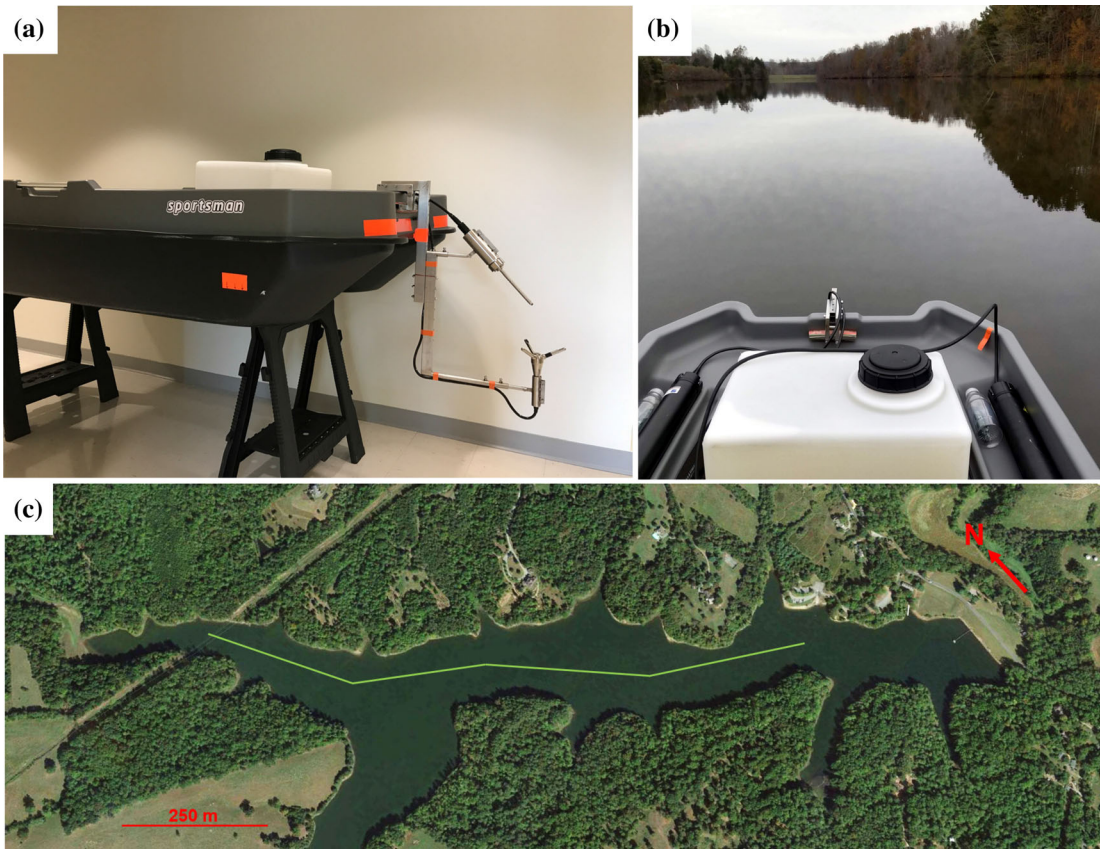

Fig. 1 Mobile measurements of air–water gas exchange in a reservoir. (**a**) Close-up look at the upward facing cabled acoustic Doppler velocimeter (ADV) and downward facing dual O_2-temperature sensor. The sensors are mounted in the bow of a two-person pontoon boat propelled by an electric trolling motor. (**b**) Measurements under calm low-wind conditions. The white container is a water filled ballast tank. The black cylinders are the ADV and its battery canister. The two smaller clear containers each hold an atmospheric pressure sensor. (**c**) Approximate path of the 1-km long transect in Beaver Creek Reservoir (Virginia) along which data were collected in this study (credits: (a) and (b) are photos by the authors, (c) is a screenshot from Google Earth).

to temperature variations and will give variable readings at the same molar O_2 concentration if the temperature changes (Gundersen et al. 1998). Thus, rapid temperature fluctuations associated with a turbulent eddy heat flux will mistakenly be recorded as fluctuations in O_2 concentration and bias the O_2 flux calculation unless a temperature correction of the O_2 signal is performed. Obviously, this correction should be based on a temperature measured in close proximity to the O_2 reading (Fig. 2). This correction can usually be ignored in benthic environments because the vertical heat flux is usually small relative to the flux of O_2 due to modestly varying mean temperatures.

The edge of the dual O_2-temperature sensor tip was positioned $\sim$ 2.0 cm "downstream" of the edge of the ADV's measuring volume so that water passed through this volume as the boat was propeller forward before sweeping over the angled O_2 sensing tip (Fig. 1a). Power was supplied from an external battery (Fig. 1b) with a capacity that allowed 64 Hz data to be collected continuously for at least 48 hr. Because all instrument components were designed for underwater use, they were not affected by rain or humid conditions.

Supporting environmental variables that were measured during deployments were used to verify recorded data and to examine the controls of derived gas-exchange rates and coefficients. These variables included mean O_2 concentration and temperature at the measuring depth ($\sim$ 10 cm) recorded every 1 min with two stable independent dual O_2-temperature sensors (miniDOT, PME). Also, local atmospheric pressure (Fig. 1b) was measured with one or two stable independent triple pressure–temperature–humidity sensors (RHT50, Extech). These measurements allowed for accurate calculation of the O_2 saturation concentration from Garcia and Gordon (1992) as a function of surface water temperature with correction for the actual atmospheric pressure.

Field tests

The new mobile application of the aquatic eddy covariance technique was tested in Beaver Creek Reservoir (Virginia). This reservoir is $\sim$ 1.5 km long, $\sim$ 150 m wide (Fig. 1c), and has a maximum depth of $\sim$ 12 m. The reservoir is moderately eutrophic with a 26 km^2 watershed composed mostly of forested (53%) and agricultural (38%) land. Three deployments were

Fig. 2 Close-up look at the tip of the robust and fast-responding dual O_2-temperature sensor developed for aquatic eddy covariance measurements. A replaceable black plastic disc contains the O_2 sensing foil, which is marked with a red circle and has a diameter of 5.0 mm. The < 1 mm shiny thermistor tip is seen below it (credits: photo by the authors).

done under calm low-wind conditions on 18 and 25 September 2017 and on 14 November 2018. Mean surface water temperature ranged from 11°C to 25°C among these deployments. Prior to data recording, a level was used to ensure that the underwater sensors were as level as possible to minimize post-processing rotations of the velocity field to correct for sensor tilt.

Calculations of eddy fluxes

Fluxes of both O_2 and sensible heat were extracted from the raw eddy covariance data following the same multistep process described below for O_2.

First, the O_2 concentration was calibrated against the stable independent dual O_2-temperature sensor data. All 64 Hz data were then averaged to 16 Hz data, which reduce noise while still providing adequate resolution to contain the full frequency spectrum carrying the flux signal (Berg et al. 2009). This assumption was validated by comparing fluxes calculated from both 16 and 64 Hz data for a subset of the data.

O_2 fluxes, one for each 3 min of traveled distance (~ 45 m), were extracted from the 16 Hz data using the software package EddyFlux version 3.3. If required, this software rotates the flow velocity field for each data segment to correct for sensor tilt (Lee et al. 2004; Lorrai et al. 2010; Lorke et al. 2013) by nullifying the transverse and the vertical mean velocities. The vertical eddy flux was then calculated as (defined positive upward):

$$J_{\text{eddy}} = \overline{w'C'} \quad (1)$$

where the overbar symbolizes the averaging over the 3-min data segment, and w' and C' are the fluctuating vertical velocity and the fluctuating O_2 concentration, respectively. These fluctuating components are calculated as $w-\bar{w}$ and $C-\bar{C}$, where w and C are measured values (at 16 Hz), and $\bar{w}$ and $\bar{C}$ are mean values defined as least square linear fits to all w and C values within the 3-min time interval, a procedure usually referred to as linear de-trending (Lee et al. 2004; Berg et al. 2009).

Due to the response time of the dual O_2-temperature sensor combined with its position "downstream" from the ADV's measuring volume, a time shift correction must be applied (Berg et al. 2016). Following the standard practice for eddy covariance data processing (Fan et al. 1990; McGinnis et al. 2008; Lorrai et al. 2010), this was done by repeating the outlined flux extraction procedure, while shifting the 16 Hz O_2 concentration data back in time, 1/16 s at a time, until the numerically largest flux was identified.

Calculations of gas exchange coefficients

Despite the complexity of processes that control air–water gas exchange, the widely used expression for its magnitude is simple and assumes conceptually that gas is transported by molecular diffusion across intact boundary layers, or thin films, on each side of the interface (Whitman 1923; Liss and Slater 1974):

$$J_{\text{air-water}} = k(C_{\text{water}} - C_{\text{air}}) \quad (2)$$

where $J_{\text{air–water}}$ is the exchange rate, or vertical flux, of the gas (positive upward), C_{water} is the gas bulk concentration below the film on the water-side, C_{air} is the concentration above the film on the air-side, and k is the gas exchange coefficient, often also referred to as the "gas transfer velocity" or "piston velocity." For most gases, C_{water} and C_{air} are straightforward to measure continuously in situ with modern autonomous sensors (Koopmans and Berg 2015; Fritzsche et al. 2017; Staudinger et al. 2018) or calculate from known relationships, whereas the complexity of gas exchange and its many controlling variables are contained entirely in k (Macintyre et al. 1995; McKenna and McGillis 2004; Cole et al. 2010).

Estimating k from Eq. 2 requires that the O_2 flux over the air–water interface is known, but the eddy flux (J_{eddy} in Eq. 1) is measured ~ 10 cm below the interface. In measurements from a stationary position, in a river for example, a correction can be applied that accounts for the O_2 stored in the water between the measuring point and the air–water interface (Berg and Pace 2017). Because any lateral variations in O_2 concentration recorded in mobile aquatic eddy covariance measurements would be misinterpreted as a change in storage, we did not apply such a correction here, and assumed to link Eq. 1 and 2 as

$$J_{\text{air-water}} = J_{\text{eddy}} \quad (3)$$

The saturation concentration of O_2 (C_{air} in Eq. 2) was calculated from Garcia and Gordon (1992) as a function of salinity (here 0 ppt) and measured surface water temperature, and then corrected for the measured atmospheric pressure using Henry's law. The water column O_2 bulk concentration (C_{water} in Eq. 2) was measured with the fast-responding dual O_2-temperature sensor and simultaneously with the stable independent dual O_2-temperature sensors. By using known values of $J_{\text{air-water}}$, C_{water}, and C_{air}, values of k were calculated from Eq. 2 for every 3 min of traveled distance ($\sim$ 45 m), and then converted to the standard gas exchange coefficients, k_{600}, for CO_2 at 20°C (Jähne et al. 1987; Wanninkhof 1992; Cole et al. 2010).

As a final step, a thorough systematic data quality check was performed on all measured data, extracted O_2 fluxes, and derived k_{600} values. Data segments with abnormalities, for example, caused by floating debris that collided with the sensors and produced erroneous or distorted data readings, were discarded. Similarly, during one deployment in particular, substantial changes in mean O_2 concentration over short distances were recorded along the transect (Fig. 1c). Such changes can distort de-trending of the fluctuating O_2 concentration and were also removed from the data record (*see* details later). The data and derived results that passed this quality check are presented below.

Results and assessments

Two examples

Figure 3 shows two 12-min data sections from two different deployments along the 1-km long transect in Beaver Creek Reservoir (Fig. 1). The surface water was slightly supersaturated in O_2 in one example (left panels, 107%) and highly undersaturated in the other (right panels, 56%).

The 3D velocity fields in the two examples (Fig. 3a,b) indicate that the ADV sensor head (Fig. 1a) was lined up as intended so that the boat's movement was registered in the *x*-direction and showed a steady mean speed of the boat of 23 and 33 cm s^{-1}, respectively. These mean velocities bracket the range used in all measurements and translate to boat movements of 41 and 59 m for each 3-min time interval used in flux extractions. The change in boat speed in the very first part of the second example (Fig. 3b) represents an acceleration at one of the ends of the traveled transect (Fig. 1c). Time intervals with such changes in velocity were left out of the flux calculations.

All 16 Hz O_2 concentration data recorded during the two examples by the fast-responding eddy sensor (Fig. 1a) agreed closely with the two stable independent sensors readings (Fig. 3c,d), and also contain no visible noise or spikes. This desirable performance was attributed to the 5.0 mm large oxygen-sensitive foil at the tip of the sensor (Fig. 2) which makes the signal readings much less susceptible than microsensors to distortion when colliding with small particulate matter floating in the water column (Berg et al. 2016). The near-constant O_2 concentration of 275.6 and 191.5 μmol L^{-1} in the two examples represents, at the measured surface water temperatures of 24.7°C and 11.2°C and the measured atmospheric pressures of 1003.1 and 1013.0 mbar, very different saturation levels of 107% and 56%.

The cumulative O_2 fluxes (Fig. 3e,f), one for each 3-min time interval used in the flux extraction, all showed clear linear trends. This desirable pattern indicates that quasi-steady gas exchange persisted for the 3-min time intervals and over the distance that was traveled during these measurement periods. The steady exchanges also document that the recorded data contained a strong statistically significant eddy flux signal (Berg et al. 2003; Berg and Pace 2017).

The direction of the 3-min based eddy fluxes of O_2 derived from Eq. 1 for the two examples (Fig. 3g,h) match the O_2 concentration differences over the air–water interface (Fig. 3c,d), and contained only little variation within each example. This latter result reflects internal consistency in the flux determination, and also, that near-perfect conditions were present during the data sampling period. The average O_2 fluxes amounted to a release from the reservoir of 11.2 ± 1.1 and an uptake of −11.6 ± 0.6 mmol m^{-2} d^{-1} (SE, n = 4) for the respective sample dates (Fig. 3g,h). Differences in gas exchange coefficient (*see* below), combined with different driving O_2 concentration differences in the two examples (Fig. 3c,d), coincidentally gave rise to fluxes of similar size but with opposite directions.

Standard gas-exchange coefficients, k_{600}, exhibited only small variations within each example (Fig. 3i,j) but had substantially different averages of 0.50 ± 0.05 and 0.092 ± 0.004 m d^{-1} (SE, n = 4). This difference is equivalent to a factor of 5 and is discussed in detail below.

The average time lag correction for both deployments was 0.4 s. Also, co-spectral analysis (not shown) for the deployments showed that the O_2 signal carrying the flux was contained well within the 3-min averaging interval.

Sensible heat fluxes, measured simultaneously with the O_2 fluxes, are shown in Fig. 4 and are obviously based on the same velocity data (Fig. 4a,b). Similarly to the O_2 data, the 16 Hz surface water temperature data (Fig. 4c,d) recorded by the fast-responding eddy sensor (Fig.1a) agreed flawlessly with the two stable independent sensors, and similarly, contain no visible noise or spikes.

The cumulative fluxes of heat (Fig. 4e,f) exhibited, similar to those for O_2, clear linear trends in both examples.

Their associated heat fluxes (Fig. 4g,h), one for each 3-min time interval, exhibited only small variations within each example. Similar to O_2, this result reflects internal consistency in the determination of heat fluxes, and their averages amounted to heat releases from the reservoir of 59.4 ± 2.5 and 15.8 ± 2.5 W m^{-2} (SE, n = 4), a difference of almost a factor of 4. The average time lag correction in the heat flux calculation

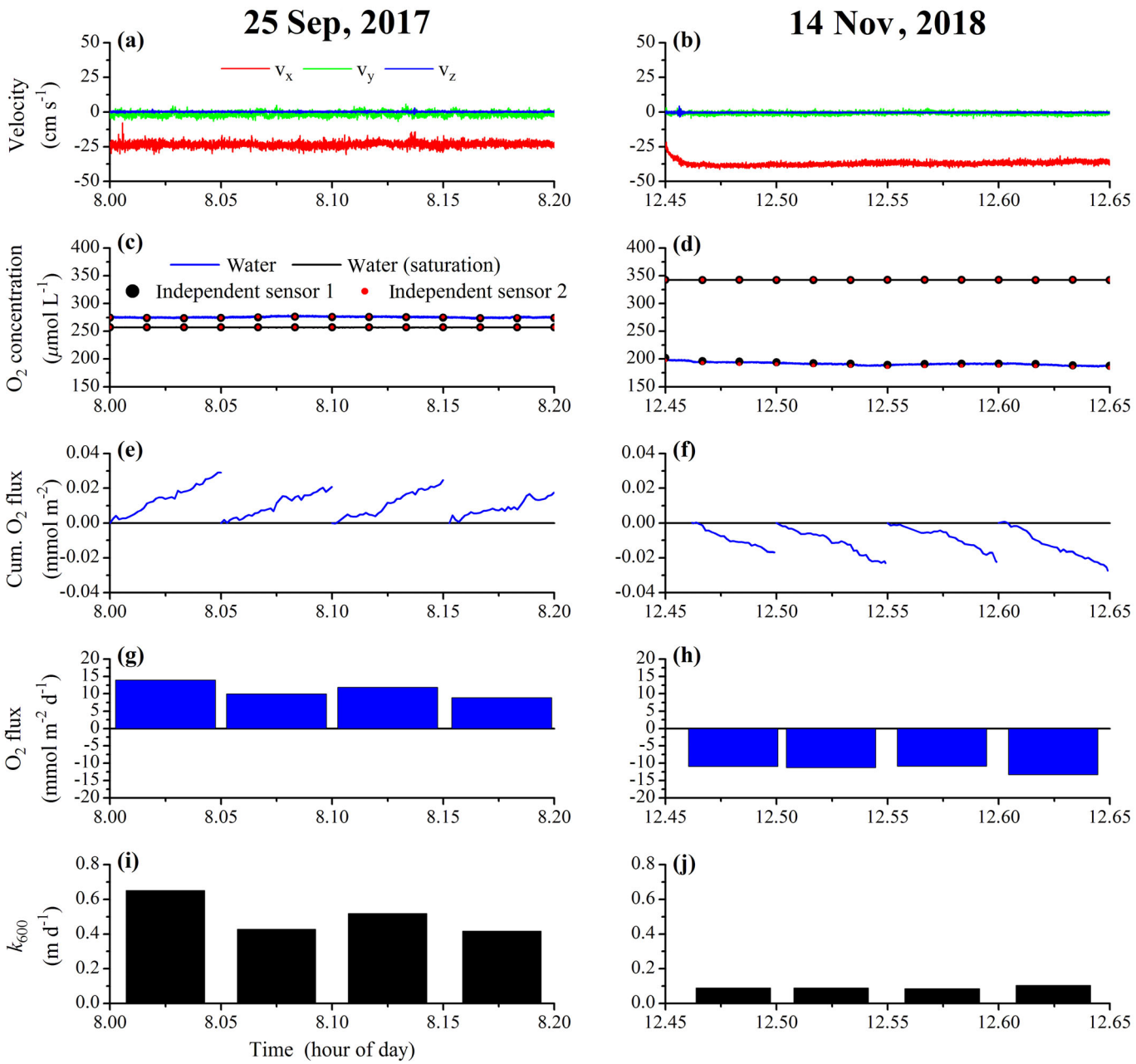

Fig. 3 Two 12-min examples of O_2 flux and gas exchange measurements from a moving boat. One deployment was done under slightly supersaturated conditions (left) and one under undersaturated conditions (right). (**a**, **b**) Three velocity components at 16 Hz (*x*, *y*, *z*; *z* is vertical). (**c**, **d**) Actual O_2 concentration at 16 Hz, saturation concentration, and the same two parameters measured with two independent sensors. (**e**, **f**) Cumulative O_2 flux over 3-min time intervals with clear linear trends indicative of a strong consistent flux signal. (**g**, **h**) O_2 flux (positive values represent a release to the atmosphere). Each flux value was extracted from 3-min of data, equivalent to movements of 41 to 59 m depending on boat speed. (**i**, **j**) Standard gas exchange coefficient (k_{600}) derived from the 3-min O_2 flux estimates.

for both deployments was 0.5 s. Similar to oxygen, co-spectral analysis for these deployments showed that the temperature signal carrying the flux is contained well within the 3-min averaging interval.

Heat fluxes of this magnitude require instantaneous temperature correction of the O_2 signal, as was done here, to avoid temperature fluctuations being recorded as fluctuations in O_2 concentration, and thus, biasing the O_2 flux calculation.

Deployment averages and their relationship

Averages from all three deployments of selected key-variables are given in Table 1. The average boat speed varied

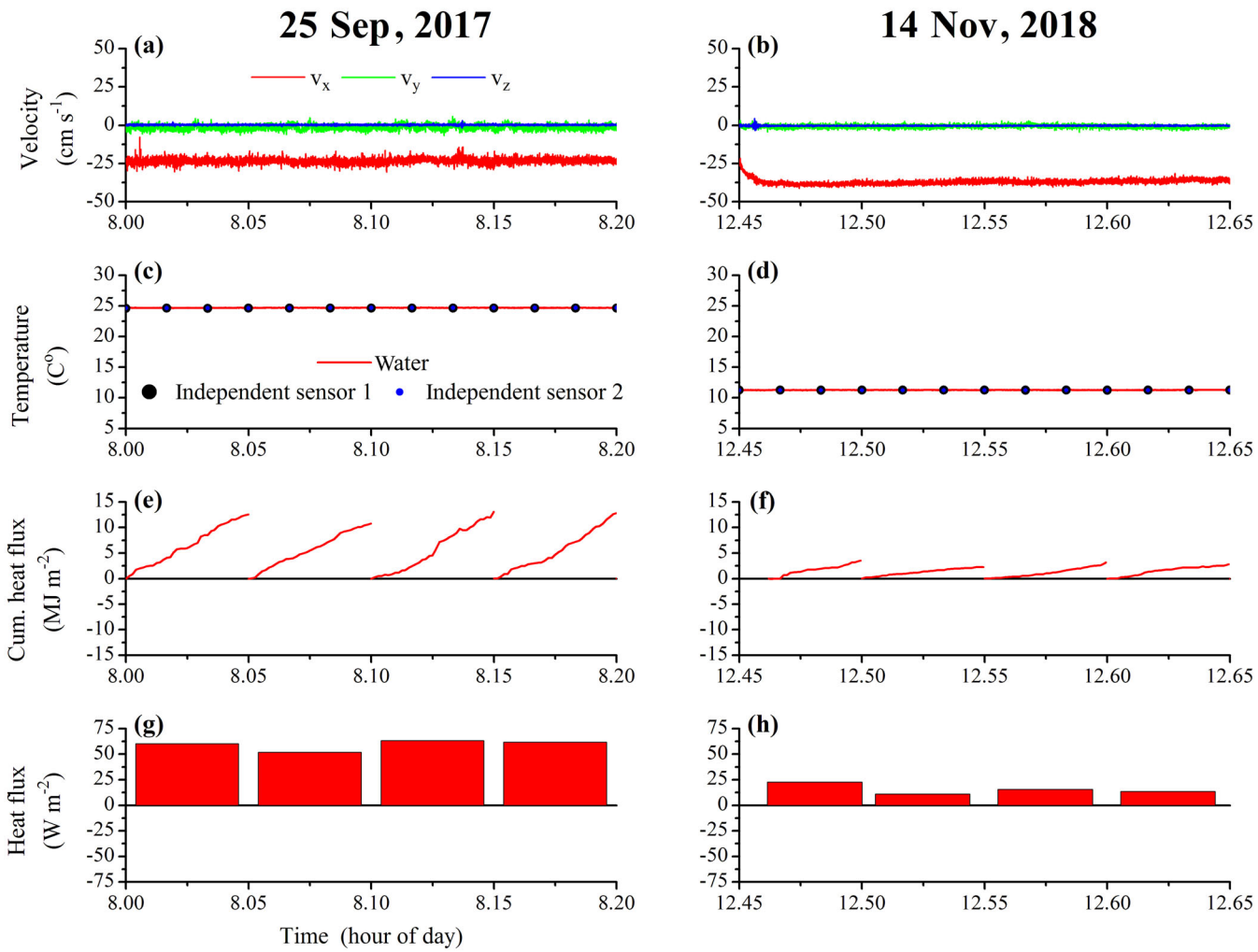

Fig. 4 Heat flux for the same two time periods as shown in Fig. 3. (**a**, **b**) Three velocity components at 16 Hz (*x*, *y*, *z*; *z* is vertical). (**c**, **d**) Water temperature at 16 Hz, and also recorded with two independent sensors. For reference, the air temperature was also measured to be 19.6°C and 7.1°C at a nearby airport during the two deployments. (**e**, **f**) Cumulative heat flux over 3-min time intervals with clear linear trends. (**g**, **h**) Heat flux (positive values represent a release). Each value was extracted from the same 3-min time intervals shown in Fig.3.

between 23.3 and 32.5 cm s^{-1}, equivalent to boat movements of 42 and 59 m per 3-min time interval. The average eddy flux of O_2 varied from a release of 9.1 mmol m^{-2} d^{-1} under slightly supersaturated conditions (107%) to an uptake of −7.8 mmol m^{-2} d^{-1} during undersaturated conditions (56%). These fluxes were driven by substantially different air–water concentration differences of 19.7 and −134.0 μmol L^{-1}. The average standard gas exchange coefficient, k_{600}, all measured under calm low-wind conditions (Fig. 1b), varied six-fold from 0.070 to 0.39 m d^{-1}. We believe this sizeable variation was mainly controlled by two variables (*see* Discussion), the air–water heat flux (Fig. 4g,h) and the temperature of the surface water, which affects its dynamic viscosity, molecular diffusivity of O_2, and thermal expansion coefficient. Values of these three variables (Table 1) were calculated according to Vogel (1921), Broecker and Peng (1974), and Kell (1975). Among the three deployments, the heat flux and water temperature varied up to 250% and 119% relative to their minimum values, and the equivalent relative values for the dynamic viscosity, molecular diffusivity of O_2, and the thermal expansion coefficient were 39%, 43%, and 138%.

Deployment averages (Table 1) of k_{600} are plotted as a function of their associated values of air–water heat flux and water temperature in Fig. 5. The plane describing these data exhibited a 0.1 m d^{-1} increase in k_{600} when the heat loss from the reservoir increased by 19.4 W m^{-2}, and similarly, when the water temperature increased 9.7°C.

Lateral variations in mean water column O_2 concentration

There was significant variation in 30-s means of the O_2 concentration in the surface water along the 1-km long transect (Fig. 1) during one deployment (14 November 2018;

Table 1. Averages of key-variables for the three proof-of-concept deployments in Beaver Creek Reservoir. All measurements were performed under calm low-wind conditions. Values of k for O_2 were converted to k_{600} according to (Cole et al. 2010).

Deployment date	n	Velocity of platform (cm s^{-1})	O_2 flux (mmol m^{-2} d^{-1})	O_2 conc. difference (µmol L^{-1})	k (m d^{-1})	k_{600} (m d^{-1})	Heat flux W (m^{-2})	Water temp. (°C)	Dynamic viscosity (mPa s)	Molecular diffusivity of O_2 (cm^2 s^{-1})	Thermal expansion coefficient (g cm^{-3} °C^{-1})
18 Sep 2017	14	25.7	4.90	15.5	0.328	0.281	29.5	23.9	0.915	22.8 10^{-6}	−2.45 10^{-4}
25 Sep 2017	15	23.3	9.09	19.7	0.463	0.391	49.7	24.5	0.902	23.2 10^{-6}	−2.50 10^{-4}
14 Nov 2018	47	32.5	−7.83	−134.0	0.0584	0.0701	14.2	11.2	1.25	16.2 10^{-6}	−1.05 10^{-4}

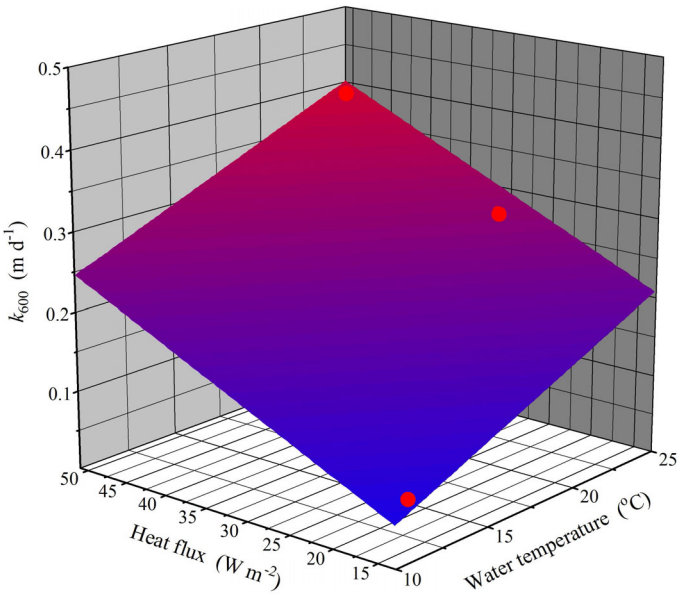

Fig. 5 Standard gas exchange coefficient, k_{600}, measured under calm low-wind conditions and plotted against the air–water heat flux and water temperature. The red dots represent deployment averages from Table 1. Values of k_{600} were controlled mainly by the air–water heat flux and the water temperature (*see* text for details).

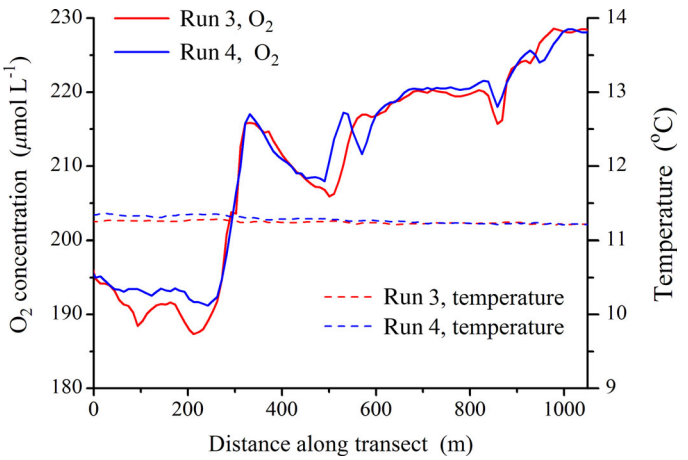

Fig. 6 Variations in O_2 concentration and temperature in the surface water along the 1-km long transect used in this study (Fig. 1). For O_2, the same > 20% variation was found repeatedly during different "runs" of the transect within the same deployment while the variation in temperature was insignificant. Such variations in O_2 can bias estimates of gas exchange and whole-system metabolism for lakes and reservoirs if based on single-point measurements.

Table 1). This variation exceeded 20% and was found consistently during different transect runs, which indicates that the pattern persisted at least for several hours (Fig. 6). Such spatial variations in O_2 concentration can bias estimates of gas exchange and whole-system metabolism if they are only based on single-point measurements (Staehr et al. 2010; Schilder et al. 2013; Holgerson et al. 2017) (*see* Discussion below).

Conversely, practically no variation was found in the corresponding temperature measurements along the transect (Fig. 6).

Discussion

Significance of study and future applications

This proof-of-concept study documents that gas exchange rates and coefficients can be determined consistently for lakes and reservoirs with near-stagnant water by applying the aquatic eddy covariance technique below the air–water interface from a moving measurements platform. We find that relative to traditional methods this new approach gives gas exchange rates and coefficients with improved precision and at a high spatial and temporal resolution, all under true in situ conditions.

In this study, we were able to measure air–water exchange of O_2 and sensible heat using well-tested fast-responding aquatic eddy covariance sensors for these variables (Berg et al. 2016). We anticipate that such O_2 fluxes will improve metabolic estimates for lakes and reservoirs, particularly under calm low-wind conditions in which widely used empirical relationships for gas exchange become increasingly uncertain or break down (Clark et al. 1995; Cole and Caraco 1998; Vachon et al. 2010).

Furthermore, reliable autonomous underwater sensors for the most important greenhouse gasses, CO_2, CH_4, and N_2O, are rapidly becoming available. While these sensors are too slow and too bulky to be used for aquatic eddy covariance, they give accurate readings of mean gas concentrations. From measured O_2 fluxes in this study, we derived standard gas exchange coefficients, k_{600}, that can easily be translated to any gas of interest. We believe that pairing such gas exchange coefficients with corresponding measurements of greenhouse gas concentrations will be a powerful way to study greenhouse gas emissions from lakes and reservoirs particularly in the context of understanding the physical, chemical, and biological processes that drive them.

Quality of data

The high quality of data that can be collected by mobile aquatic eddy covariance is exemplified in the two 12-min sections of data (Figs. 3, 4) from two different deployments along the 1 km transect in a reservoir (Fig. 1), one slightly supersaturated in O_2 (107%) and one highly undersaturated (56%). These data, for both O_2 and temperature, are of comparable quality and internal consistency to those published for many benthic environments (Long et al. 2013; Attard et al. 2015; Berg et al. 2019). Specifically, all 16 Hz data were recorded with low noise and free of spikes, and the O_2 concentrations and temperatures matched the reading of the stable independent sensors (Figs. 3, 4). Also, all cumulative fluxes had clear linear trends, indicating a strong and consistent flux signal contained in the data. Finally, all individual O_2 and heat fluxes and k_{600} values, each derived from very short 3-min time intervals (Figs. 3, 4), matched one another well within each deployment.

Comparisons to empirical relationships for k_{600}

In a recent comparison for a boreal lake, Heiskanen et al. (2014) calculated k_{600} values of 0.089, 0.091, 0.52, 0.80, and 2.0 m d^{-1} in the 0 to 1 m s^{-1} range of wind speeds using empirical relationships given by Wanninkhof (1992), Crusius and Wanninkhof (2003), Cole and Caraco (1998), McGillis et al. (2001), and McGillis et al. (2004). Although some of these regressions were originally derived for marine environments, they are frequently used indiscriminately, as here, for other types of aquatic systems. This extreme example by Heiskanen et al. (2014), illustrates how widely such estimates of k_{600} values can vary at low-wind conditions. Even when narrowing in on some of the most popular relationships by Cole and Caraco (1998) and Crusius and Wanninkhof (2003), developed specifically for small lakes (0.15 and 0.13 km^2) and low wind speed (< 9 and 6 m s^{-1}), large variations are seen in their predictions. At wind speeds of 0, 1, and 2 m s^{-1}, which likely match conditions during our study, the Cole and Caraco regression yields k_{600} values of 0.50, 0.55, and 0.66 m d^{-1}, respectively, whereas the Crusius and Wanninkhof relationship for the same wind speeds predicts significantly lower values of 0.040, 0.095, and 0.29 m d^{-1}. All k_{600} values produced by direct mobile aquatic eddy covariance measurements in this study fall within the range of these two widely used empirical relationships for small freshwater systems and low-wind conditions.

Dependency of gas exchange on heat flux and water temperature

Deployment averages of k_{600} correlate strongly with their corresponding heat fluxes and mean surface water temperatures (Fig. 5). The latter was found even though the widely used expression for k_{600} that we adopted from Cole et al. (2010) does include a temperature correction through the non-dimensional Schmidt number (ratio between the temperature dependent kinematic viscosity and molecular diffusivity). Although this expression for k_{600} was found to be specifically valid for low-wind conditions by Cole et al. (2010), it may not adequately account for variations in temperature in field situations as we encountered here.

The heat flux and surface water temperature are not fully independent variables, but they affect gas exchange through separate processes. Heat fluxes that cool the surface water drive convective water movements and, especially under calm low-wind conditions, this movement is known to affect gas exchange (Bannerjee and MacIntyre 2004; MacIntyre et al. 2010). Water temperature affects several properties of water that impact gas exchange, most notably the dynamic viscosity, molecular diffusivity of O_2, and thermal expansion coefficient. Just within the temperature span encountered

here, from 11.2°C to 24.5°C, these three variables changed 39%, 43%, and 138% from their minimum values (Table 1), and while corrections for the first two are included in the Cole et al. (2010) expression, the last, and by far the largest one, is not. This is likely the explanation for the strong dependency of k_{600} on the mean surface water temperature. For example, a larger thermal expansion coefficient due to a higher water temperature will, at the same sized heat flux, cool the surface water, trigger a significantly larger density stratification, and drive a more substantial convective flow. This will in turn lead to an increase in k_{600}, beyond what is included in the Cole et al. (2010) expression, but is fully in line with our findings (Fig. 5).

Lateral variations in mean water column O_2 concentration

The significant lateral variation observed in mean surface water O_2 concentration that exceeded 20% (Fig. 6) during a deployment along our 1-km long transect (Fig. 1) likely reflects variation in biological processes. No lateral variation was measured in the corresponding temperatures that potentially could affect calculation of C_{air} in Eq. 2, and there was no clear pattern in k_{600} along the transect. Lateral variation in variables such as the O_2 concentration is common in lakes and reservoirs in transition from lotic to lentic conditions and often reflects a shift in relative heterotrophic vs. autotrophic activity (Kimmel and Groeger 1984; Kalff 2002).

Because the concentration difference driving gas exchange (Eq. 2) is often small (Table 1), lateral variations in O_2 concentration in the surface water can result in considerable variations in gas exchange, even over very short distances. It is even plausible that air–water exchange of O_2 at times can have opposite directions along a transect if different areas of a water body are under- and supersaturated. Our results underline the findings from earlier studies that accurate whole-system gas exchange and metabolic assessments can be improved with multiple sensors deployed in carefully chosen locations (Staehr et al. 2010; Van de Bogert et al. 2012; Schilder et al. 2013). As autonomous sensors are decreasing considerably in cost and are becoming widely available, it should be possible for more studies to incorporate such lateral variations.

As a side note, extreme lateral O_2 concentration differences over short distances (Fig. 6) can complicate aquatic eddy flux extractions because linear detrending, as was used here (Eq. 1), may not adequately describe the variation in mean O_2 concentration through the 3-min time interval used for each flux calculation. However, more advance detrending schemes exist and can be considered under such conditions (Lee et al. 2004; Reimers et al. 2012; Berg et al. 2013).

Comments and recommendations

Based on our proof-of-concept test, mobile aquatic eddy covariance can help reduce the widely recognized problem of large uncertainties of gas exchange estimates for lakes and reservoirs. Given its noninvasive nature, precision, and high spatial and temporal resolution, this approach is a promising means to study the dynamics and controls of gas exchange under in situ conditions. A natural "next step" would be to compare the new approach with one or two traditional methods, all deployed simultaneously and under different conditions, including full diel cycles and a wide range of different O_2 saturation levels and temperatures. Such a follow-up study would reveal more specific information on the strengths and weaknesses of all approaches.

Some aspects of the new mobile approach can likely be adjusted and optimized, but based on our first tests, we recommend using a boat speed of about 25 cm s^{-1} as this is adequate for maneuvering a heavy, low-sitting boat and, at the same time, obtaining a very good resolution of the "eddies" carrying the flux signal in the surface water. We also recommend that data are measured no more than 10 to 15 cm below the air–water interface to obtain a representation of the air–water exchange as directly as possible. Because the absolute mean O_2 concentration is used to estimate k_{600}, it is furthermore important that the stable independent O_2 sensors are accurately calibrated to give precise readings. Finally, we stress that simultaneous rapid temperature measurements should be performed within a few mm of the O_2 recordings to allow instant temperature corrections of the O_2 signal.

The preferred mobile platform used here (Fig. 1) can be easily reproduced as it relies exclusively on standard materials and commercially available instrumentation. However, to obtain the best quality data, also when the weather conditions are not as calm as in our test deployments, a larger and heavier boat should be used. A double hulled boat with the aquatic eddy covariance instrumentation mounted on one hull and propelled by a bow mounted programmable GPS-controlled electric trolling motor on the other hull appears to be a highly attractive solution.

References

Attard, K. M., I. F. Rodil, R. N. Glud, P. Berg, J. Norkko, and A. Norkko. 2019. Seasonal ecosystem metabolism across shallow benthic habitats measured by aquatic eddy covariance. Limnol. Oceanogr.: Letters **4**(3): 79–86. doi: 10.1002/lol2.10107.

Attard, K. M., H. Stahl, N. A. Kamenos, G. Turner, H. L. Burdett, and R. N. Glud. 2015. Benthic oxygen exchange in a live coralline algal bed and an adjacent sandy habitat: An eddy covariance study. Mar. Ecol. Prog. Ser. **535**: 99–115.

Bannerjee, S., and S. MacIntyre. 2004. The air–water interface: Turbulence and scalar interchange, p. 181–237. *In* Advances in coastal and ocean engineering, v. **9**. World Scientific.

Bastviken, D., L. J. Tranvik, J. A. Downing, P. M. Crill, and A. Enrich-Prast. 2011. Freshwater methane emissions offset the continental carbon sink. Science **331**: 50–50.

Battin, T. J., S. Luyssaert, L. A. Kaplan, A. K. Aufdenkampe, A. Richter, and L. J. Tranvik. 2009. The boundless carbon cycle. Nat. Geosci. **2**: 598–600.

Berg P., M. L. Delgard, P. Polsenaere, K. J. McGlathery, S. C. Doney, and A. C. Berger. 2019. Dynamics of benthic metabolism, O2, and pCO2in a temperate seagrass meadow. Limnology and Oceanography. **64**: 2586–2604. doi: 10.1002/lno.11236.

Berg, P., M. L. Delgard, R. N. Glud, M. Huettel, C. E. Reimers, and M. L. Pace. 2017. Non-invasive flux measurements at the benthic interface: The aquatic Eddy covariance technique. Limnol. Oceanogr.: e-Lectures **7**: 1–50. doi:10.1002/loe2.10005

Berg, P., R. N. Glud, A. Hume, H. Stahl, K. Oguri, V. Meyer, and H. Kitazato. 2009. Eddy correlation measurements of oxygen uptake in deep ocean sediments. Limnol. Oceanogr.: Methods **7**: 576–584.

Berg, P., D. Koopmans, M. Huettel, H. Li, K. Mori, and A. Wüest. 2016. A new robust dual oxygen-temperature sensor for aquatic eddy covariance measurements. Limnol. Oceanogr.: Methods **14**: 151–167.

Berg, P., M. H. Long, M. Huettel, J. E. Rheuban, K. J. McGlathery, R. W. Howarth, K. H. Foreman, A. E. Giblin, and R. Marino. 2013. Eddy correlation measurements of oxygen fluxes in permeable sediments exposed to varying current flow and light. Limnol. Oceanogr. **58**: 1329–1343.

Berg, P., and M. L. Pace. 2017. Continuous measurement of air–water gas exchange by underwater eddy covariance. Biogeosciences **14**: 5595–5606.

Berg, P., H. Roy, F. Janssen, V. Meyer, B. B. Jorgensen, M. Huettel, and D. de Beer. 2003. Oxygen uptake by aquatic sediments measured with a novel non-invasive eddy-correlation technique. Mar. Ecol. Prog. Ser. **261**: 75–83.

Berg, P., H. Roy, and P. L. Wiberg. 2007. Eddy correlation flux measurements: The sediment surface area that contributes to the flux. Limnol. Oceanogr. **52**: 1672–1684.

Billett, M., and T. Moore. 2008. Supersaturation and evasion of CO_2 and CH_4 in surface waters at Mer Bleue peatland, Canada. Hydrol. Process. **22**: 2044–2054.

Borges, A. V., B. Delille, L. S. Schiettecatte, F. Gazeau, G. Abril, and M. Frankignoulle. 2004. Gas transfer velocities of CO_2 in three European estuaries (Randers Fjord, Scheldt, and Thames). Limnol. Oceanogr. **49**: 1630–1641.

Broecker, W. S., and T.-H. Peng. 1974. Gas exchange rates between air and sea. Tellus **26**: 21–35.

Clark, J. F., P. Schlosser, R. Wanninkhof, H. J. Simpson, W. S. Schuster, and D. T. Ho. 1995. Gas transfer velocities for SF6 and ^{3}He in a small pond at low wind speeds. Geophys. Res. Lett. **22**: 93–96.

Cole, J. J., D. L. Bade, D. Bastviken, M. L. Pace, and M. Van de Bogert. 2010. Multiple approaches to estimating air-water gas exchange in small lakes. Limnol. Oceanogr.: Methods **8**: 285–293.

Cole, J. J., and N. F. Caraco. 1998. Atmospheric exchange of carbon dioxide in a low-wind oligotrophic lake measured by the addition of SF6. Limnol. Oceanogr. **43**: 647–656.

Cole, J. J., Y. T. Prairie, N. F. Caraco, W. H. McDowell, L. J. Tranvik, R. G. Striegl, C. M. Duarte, P. Kortelainen, J. A. Downing, J. J. Middelburg, and J. Melack. 2007. Plumbing the global carbon cycle: Integrating inland waters into the terrestrial carbon budget. Ecosystems **10**: 171–184.

Crusius, J., and R. Wanninkhof. 2003. Gas transfer velocities measured at low wind speed over a lake. Limnol. Oceanogr. **48**: 1010–1017.

Czikowsky, M. J., S. MacIntyre, E. W. Tedford, J. Vidal, and S. D. Miller. 2018. Effects of wind and buoyancy on carbon dioxide distribution and air-water flux of a stratified temperate lake. J. Geophys. Res. Biogeo. **123**: 2305–2322.

Dugan, H. A., R. I. Woolway, A. B. Santoso, J. R. Corman, A. Jaimes, E. R. Nodine, V. P. Patil, J. A. Zwart, J. A. Brentrup, and A. L. Hetherington. 2016. Consequences of gas flux model choice on the interpretation of metabolic balance across 15 lakes. Inland Waters **6**: 581–592.

Fan, S. M., S. C. Wofsy, P. S. Bakwin, D. J. Jacob, and D. R. Fitzjarrald. 1990. Atmosphere-biosphere exchange of CO_2 and O_3 in the central Amazon forest. J. Geophys. Res. Atmos. **95**: 16851–16864.

Fritzsche, E., P. Gruber, S. Schutting, J. P. Fischer, M. Strobl, J. D. Müller, S. M. Borisov, and I. Klimant. 2017. Highly sensitive poisoning-resistant optical carbon dioxide sensors for environmental monitoring. Anal. Methods **9**: 55–65.

Garcia, H. E., and L. I. Gordon. 1992. Oxygen solubility in seawater: Better fitting equations. Limnol. Oceanogr. **37**: 1307–1312.

Gundersen, J. K., N. B. Ramsing, and R. N. Glud. 1998. Predicting the signal of O-2 microsensors from physical dimensions, temperature, salinity, and O-2 concentration. Limnol. Oceanogr. **43**: 1932–1937.

Hanson, P. C., A. I. Pollard, D. L. Bade, K. Predick, S. R. Carpenter, and J. A. Foley. 2004. A model of carbon evasion and sedimentation in temperate lakes. Glob. Chang. Biol. **10**: 1285–1298.

Heiskanen, J. J., I. Mammarella, S. Haapanala, J. Pumpanen, T. Vesala, S. MacIntyre, and A. Ojala. 2014. Effects of cooling and internal wave motions on gas transfer coefficients in a boreal lake. Tellus B: Chem. Phys. Meteorol. **66**: 22827.

Holgerson, M. A., E. R. Farr, and P. A. Raymond. 2017. Gas transfer velocities in small forested ponds. J. Geophys. Res. Biogeo. **122**: 1011–1021.

Jähne, B., K. O. Münnich, R. Bösinger, A. Dutzi, W. Huber, and P. Libner. 1987. On the parameters influencing air-water gas exchange. J. Geophys. Res. Oceans **92**: 1937–1949.

Jonsson, A., J. Åberg, A. Lindroth, and M. Jansson. 2008. Gas transfer rate and CO_2 flux between an unproductive lake and the atmosphere in northern Sweden: J. Geophys. Res.: Biogeoscie. **113**: G04006, doi:04010.01029/02008JG000688.

Kalff, J. 2002. Limnology: Inland water ecosystems. Prentice Hall.

Kell, G. S. 1975. Density, thermal expansivity, and compressibility of liquid water from 0 deg to 150 deg. Correlations and tables for atmospheric pressure and saturation reviewed and expressed on 1968 temperature scale. J. Chem. Eng. Data **20**: 97–105.

Kimmel, B. L., and A. W. Groeger. 1984. Factors controlling primary production in lakes and reservoirs: A perspective. Lake Reservoir Manag. **1**: 277–281.

Koopmans, D. J., and P. Berg. 2015. Stream oxygen flux and metabolism determined with the open water and aquatic eddy covariance techniques. Limnol. Oceanogr. **60**: 1344–1355.

Kuwae, T., K. Kamio, T. Inoue, E. Miyoshi, and Y. Uchiyama. 2006. Oxygen exchange flux between sediment and water in an intertidal sandflat, measured in situ by the eddy-correlation method. Mar. Ecol. Prog. Ser. **307**: 59–68.

Lee, X., W. Massman, and B. Law. 2004. Handbook of micrometeorology: A guide for surface flux measurement and analysis. Kluwer Academic Publishers.

Liss, P., and P. Slater. 1974. Flux of gases across the air-sea interface. Nature **247**: 181–184.

Long, M. H., P. Berg, D. de Beer, and J. C. Zieman. 2013. In situ coral reef oxygen metabolism: An eddy correlation study. PLoS One **8**: e58581. doi:10.51371/journal.pone.0058581

Long, M. H., M. A. Charette, W. R. Martin, and D. C. McCorkle. 2015. Oxygen metabolism and pH in coastal ecosystems: Eddy covariance hydrogen ion and oxygen exchange system (ECHOES). Limnol. Oceanogr.: Methods **13**: 438–450.

Lorke, A., D. F. McGinnis, and A. Maeck. 2013. Eddy-correlation measurements of benthic fluxes under complex flow conditions: Effects of coordinate transformations and averaging time scales. Limnology and Oceanography: Methods. **11**: 425–437. doi: 10.4319/lom.2013.11.425.

Lorrai, C., D. F. McGinnis, P. Berg, A. Brand, and A. Wüest. 2010. Application of oxygen eddy correlation in aquatic systems. J. Atmos. Oceanic Tech. **27**: 1533–1546.

MacIntyre, S., A. Jonsson, M. Jansson, J. Aberg, D. E. Turney, and S. D. Miller. 2010. Buoyancy flux, turbulence, and the gas transfer coefficient in a stratified lake. Geophys. Res. Lett. **37**: L24604.

Macintyre, S., R. Wanninkhof, and J. P. Chanton. 1995. Trace gas exchange across the air-water interface in freshwater and coastal marine environments, p. 52–97. *In* R. C. Harriss and P. A. Matson [eds.], Biogenic trace gases: Measuring emissions from soil and water. Blackwell Science Ltd.

Mammarella, I., A. Nordbo, Ü. Rannik, S. Haapanala, J. Levula, H. Laakso, A. Ojala, O. Peltola, J. Heiskanen, J. Pumpanen, and T. Vesala. 2015. Carbon dioxide and energy fluxes over a small boreal lake in southern Finland. J. Geophys. Res.: Biogeosci. **2014**: JG002873.

Marino, R., and R. W. Howarth. 1993. Atmospheric oxygen-exchange in the Hudson River - dome measurements and comparison with other natural-waters. Estuaries **16**: 433–445.

McGillis, W. R., J. Edson, J. Hare, and C. Fairall. 2001. Direct covariance air-sea CO_2 fluxes. J. Geophys. Res. Oceans **106**: 16729–16745.

McGillis, W. R., J. B. Edson, C. J. Zappa, J. D. Ware, S. P. McKenna, E. A. Terray, J. E. Hare, C. W. Fairall, W. Drennan, and M. Donelan. 2004. Air-sea CO_2 exchange in the equatorial Pacific. J. Geophys. Res. Oceans **109**. C08S02.

McGinnis, D. F., P. Berg, A. Brand, C. Lorrai, T. J. Edmonds, and A. Wüest. 2008. Measurements of eddy correlation oxygen fluxes in shallow freshwaters: Towards routine applications and analysis. Geophys. Res. Lett. **35**: L04403.

McKenna, S., and W. McGillis. 2004. The role of free-surface turbulence and surfactants in air–water gas transfer. Int. J. Heat Mass Transf. **47**: 539–553.

Raymond, P., and J. Cole. 2001. Gas exchange in rivers and estuaries: Choosing a gas transfer velocity. Estuaries **24**: 312–317.

Raymond, P. A., J. Hartmann, R. Lauerwald, S. Sobek, C. McDonald, M. Hoover, D. Butman, R. Striegl, E. Mayorga, C. Humborg, P. Kortelainen, H. Durr, M. Meybeck, P. Ciais, and P. Guth. 2013. Global carbon dioxide emissions from inland waters. Nature **503**: 355–359.

Raymond, P. A., C. J. Zappa, D. Butman, T. L. Bott, J. Potter, P. Mulholland, A. E. Laursen, W. H. McDowell, and N. D. 2012. Scaling the gas transfer velocity and hydraulic geometry in streams and small rivers. Limnol. Oceanogr.: Fluids Environ. **2**: 41–53.

Read, J. S., D. P. Hamilton, A. R. Desai, K. C. Rose, S. MacIntyre, J. D. Lenters, R. L. Smyth, P. C. Hanson, J. J. Cole, and P. A. Staehr. 2012. Lake-size dependency of wind shear and convection as controls on gas exchange. Geophys. Res. Lett. **39**. L09405.

Reed, D. E., H. A. Dugan, A. L. Flannery, and A. R. Desai. 2018. Carbon sink and source dynamics of a eutrophic deep lake using multiple flux observations over multiple years. Limnol. Oceanogr.: Letters **3**: 285–292.

Reimers, C. E., T. Özkan-Haller, P. Berg, A. Devol, K. McCann-Grosvenor, and R. D. Sanders. 2012. Benthic oxygen consumption rates during hypoxic conditions on the Oregon continental shelf: Evaluation of the eddy correlation method. J. Geophys. Res. **117**: 1–18.

Rheuban, J. E., and P. Berg. 2013. The effects of spatial and temporal variability at the sediment surface on aquatic

eddy correlation flux measurements. Limnol. Oceanogr.: Methods **11**: 351–359.

Schilder, J., D. Bastviken, M. van Hardenbroek, P. Kankaala, P. Rinta, T. Stötter, and O. Heiri. 2013. Spatial heterogeneity and lake morphology affect diffusive greenhouse gas emission estimates of lakes. Geophys. Res. Lett. **40**: 5752–5756.

Staehr, P. A., D. Bade, M. C. Van de Bogert, G. R. Koch, C. Williamson, P. Hanson, J. J. Cole, and T. Kratz. 2010. Lake metabolism and the diel oxygen technique: State of the science. Limnol. Oceanogr.: Methods **8**: 628–644.

Staudinger, C., M. Strobl, J. P. Fischer, R. Thar, T. Mayr, D. Aigner, B. J. Müller, B. Müller, P. Lehner, and G. Mistlberger. 2018. A versatile optode system for oxygen, carbon dioxide, and pH measurements in seawater with integrated battery and logger. Limnol. Oceanogr.: Methods **16**: 459–473.

Tranvik, L. J., J. A. Downing, J. B. Cotner, S. A. Loiselle, R. G. Striegl, T. J. Ballatore, P. Dillon, K. Finlay, K. Fortino, L. B. Knoll, P. L. Kortelainen, T. Kutser, S. Larsen, I. Laurion, D. M. Leech, S. L. McCallister, D. M. McKnight, J. M. Melack, E. Overholt, J. A. Porter, Y. Prairie, W. H. Renwick, F. Roland, B. S. Sherman, D. W. Schindler, S. Sobek, A. Tremblay, M. J. Vanni, A. M. Verschoor, E. von Wachenfeldt, and G. A. Weyhenmeyer. 2009. Lakes and reservoirs as regulators of carbon cycling and climate. Limnol. Oceanogr. **54**: 2298–2314.

Vachon, D., Y. T. Prairie, and J. J. Cole. 2010. The relationship between near-surface turbulence and gas transfer velocity in freshwater systems and its implications for floating chamber measurements of gas exchange. Limnol. Oceanogr. **55**: 1723–1732.

Van de Bogert, M. C., D. L. Bade, S. R. Carpenter, J. J. Cole, M. L. Pace, P. C. Hanson, and O. C. Langman. 2012. Spatial heterogeneity affects estimates of ecosystem metabolism in two northern lakes. Limnol. Oceanogr. **57**: 1689–1700.

Van de Bogert, M. C., S. R. Carpenter, J. J. Cole, and M. L. Pace. 2007. Assessing pelagic and benthic metabolism using free water measurements. Limnol. Oceanogr.: Methods **5**: 145–155.

Vogel, H. 1921. The law of the relation between the viscosity of liquids and the temperature. Phys. Z **22**: 645–646.

Wanninkhof, R. 1985. Kinetic fractionation of the carbon isotopes ^{13}C and ^{12}C during transfer of CO_2 from air to seawater. Tellus B **37**: 128–135.

Wanninkhof, R. 1992. Relationship between wind speed and gas exchange over the ocean. J. Geophys. Res. Oceans **97**: 7373–7382.

Whitman, W. G. 1923. The two film theory of gas absorption. Chem. Metall. Eng. **29**: 146–148.

Wilkinson, G. M., C. D. Buelo, J. J. Cole, and M. L. Pace. 2016. Exogenously produced CO_2 doubles the CO_2 efflux from three north temperate lakes. Geophys. Res. Lett. **43**: 1996–2003.

Acknowledgments

This study was supported by grants from the National Science Foundation (OCE-1550822, OCE-1824144) and the University of Virginia. We thank Rachel E. Michaels for editorial assistance with the manuscript.

Submitted 05 January 2020
Revised 20 May 2020
Accepted 02 June 2020

Associate editor: Mike DeGrandpre